11th World Congress on Computational Mechanics (WCCM XI)
5th European Conference on Computational Mechanics (ECCM V)
6th European Conference on Computational Fluid Dynamics (ECFD VI)
E. Oñate, J. Oliver and A. Huerta (Eds)

INCIPIENT MOTION FOR NON–COHESIVE SEDIMENT ELLIPSOIDAL PARTICLES BY THE DISCRETE ELEMENT METHOD (DEM)

R. Bravo*, P. Ortiz* and J.L Pérez–Aparicio†

* University of Granada, Esc. Ing. Caminos.
Campus Fuentenueva. 18071 Granada, Spain
e-mail: rbravo@ugr.es, portiz@ugr.es

† Dep. of Continuum Mechanics and theory of Structures
Universitat Politécnica de Valéncia
46022 Valencia, Spain
e-mail: jopeap@upvnet.upv.es

Key words: Sediments, Ellipsoidal particles, Shields diagram, Discrete Element Method

Abstract. This work studies the initiation of motion for sediment ellipsoidal particles under the action of laminar and turbulent flows. An analytical and a numerical approach compute the motion of the particle for different conditions establishing a relationship between the Reynolds number $Re^\star$ of the flow and the non-dimensional critical shear stress $\tau^\star$ (Shields diagram). Previous formulations have not been developed for ellipsoidal particles and therefore do not fully simulate variety of shapes included in the main experimental contribution of [7], that shows a dispersion due to the variety of shapes and orientation of the particles.

Numerical and analytical approximations calculate the initiation of motion due to new drag and lift forces developed by [5] for inclined ellipsoids. The discrete element method (DEM) ([6]) is used in the numerical approach, since it is able to simulate the motion of the ellipsoids taking into account the contact interactions. Additionally, DEM computes the evolution of motion giving realistic results and reproducing the experimental results of [7] for a variety of conditions.

1 Introduction

The analysis of the conditions for the motion of a particle in a sedimentary bed under the action of a flow is a topic of long research treated since the experiments of Shields [7] to, e.g., analytical works of Dey [3] or numerical simulation based on the Discrete Element Method (DEM) by Bravo et. al. [1]. These works address a relationship for a non-dimensional critical shear stress $\tau^\star$ (Shields diagram) in terms of the friction Reynolds

number $Re^\star$, considering the sediment grains as spherical particles. The experimental results show a scattering mainly due to an ambiguous definition of the threshold condition, dependent on the shape of the particles, compactness and orientation.

Scant research has been produced in analytical and numerical formulations for the initiation of motion of non spherical particles. In this work we study the initiation of motion of ellipsoidal particles by novel analytical and numerical approaches. The analytical method considers the equilibrium of an ellipsoidal particle resting on a rough sediment bed and computes the critical shear stress for the starting motion by rolling or sliding. The numerical procedure simulates the starting motion by the DEM, introducing an aggregate of particles as sedimentary bed (see Fig. 1). Initiation of motion is examined taking into account frictional contact interaction with the bottom particles. Additionally, DEM computes the evolution of motion after breakage of equilibrium. The resulting approaches consider a more realistic configuration than the previous works: a realistic representation of the geometrical arrangement of non-cohesive particles. The geometrical configuration is complemented by a detailed representation of the distribution of stresses transmitted by the fluid flow on ellipsoidal particles, see [5].

As a summary of the main goal of this work, a relationship $Re^\star$–$\tau^\star$ (Shields diagram) as function of the size of the axes and inclinations of the ellipsoid is produced by the use of analytical and numerical methodologies. The results fit with the scattering of the experimental data of [7]. The DEM produces more realistic results than the analytical since it is able to capture stresses that produce the subsequent breakage of the equilibrium of the particle.

2 Analytical model

The model for the initiation of motion of a single ellipsoidal particle resting on the bed is defined by the bottom layer. This is a two dimensional layer with two rows of particles (left Fig. 1) and modeled as a repetition of the periodic pattern shown in right Fig. 1. The lower row is composed by fixed cylinders(e.g. [10]) that are numerically constrained by lateral boundaries (represented in right Fig. 1). A randomly oriented set of ellipsoidal particles with an initial stable orientation but able to move forms the top layer. The particles on the bottom row partially restricts motion of the ellipsoid located on the top.

The particles on the bottom are cylinder of radius R and the ellipsoids are considered as ellipsoids of revolution with axes defined by the semi–axes a, $b = c$, and by α, angle of inclination of the largest axis of the ellipsoidal particle (see Fig. 2, left and right). The length of the semi–axes are related by the parameter f, then $b = a \cdot f$ and $c = a \cdot f$. The rest of the geometrical variables depicted in Fig. 2–entrainment angles β_{12}, β_{13}, angles γ_{12}, γ_{13}, and distances d_{12}, d_{13}–are obtained imposing simple geometric relations. Ellipsoidal particle initiates its motion by sliding or by rolling. In case of sliding there is a second situation called *special case* that gives rise to particle detachment from point $\boldsymbol{B}$ and its sliding over cylinder ② (Fig. 2 left). This situation will be discussed in detail in the numerical experiments.

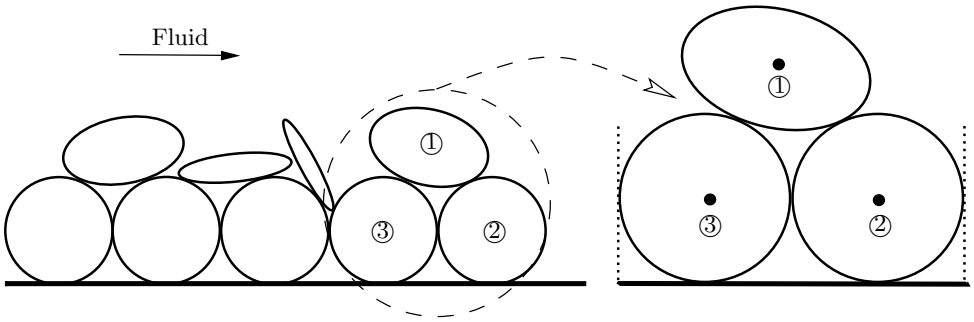

Figure 1: Sediment bed composed by the repetition of a simple pattern of cylinders and a series of ellipsoids on the top with stable orientation (right)

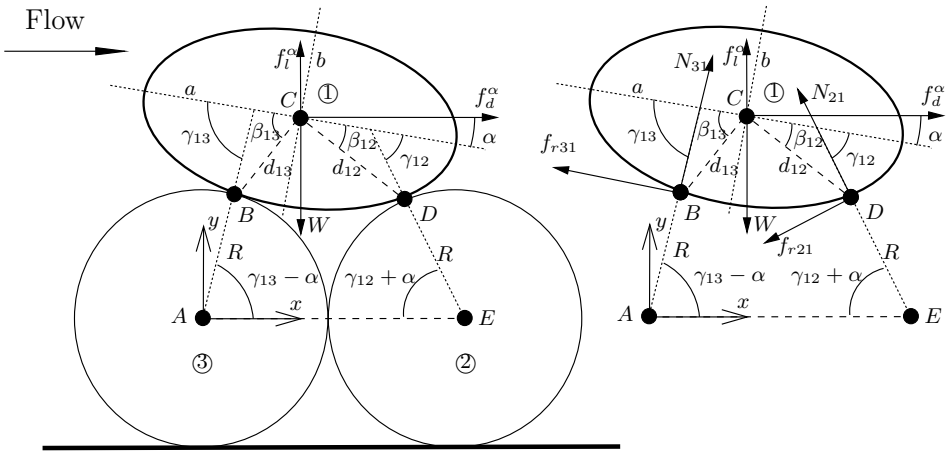

Figure 2: Forces acting on particle (left), submerged weight W, drag force f_d^α, lift force f_l^α, (right) normal contact forces $|\boldsymbol{N}_{21}|$, $|\boldsymbol{N}_{31}|$ and friction contact forces $|\boldsymbol{f}_{r21}|$ and $|\boldsymbol{f}_{r31}|$.

Considering a Cartesian coordinate system (x, y) such that x (horizontal) positive axis is aligned with the flow direction, the balance equations give the drag force $\boldsymbol{f}_d^\alpha$ in terms of lift force $\boldsymbol{f}_l^\alpha$, weight $\boldsymbol{W}$ and variables A and B (or its combination K, containing the geometrical parameters of the Fig. 2 and the friction angle ϕ).

$$|\boldsymbol{f}_{di}^\alpha| = \frac{(|\boldsymbol{f}_{li}^\alpha| - |\boldsymbol{W}|)A_i}{B_i} = (|\boldsymbol{f}_{li}^\alpha| - |\boldsymbol{W_i}|)K_i \tag{1}$$

where i is a subscript that is equal to r for rolling, s for sliding and sc for the second case of sliding *special case*. The initiation of motion occurs for the minimum value of the force $\left|\boldsymbol{f}_{d-l}^\alpha\right|=|\boldsymbol{f}_d^\alpha + \boldsymbol{f}_l^\alpha|$ of the three above equations.

Drag and lift forces are given by

$$|\boldsymbol{f}_d^\alpha| = \frac{C_d^\alpha}{2} S_{ep}\rho_f {V_f^\alpha}^2 \ , \quad |\boldsymbol{f}_l^\alpha| = \frac{C_l^\alpha}{2} S_{ep}\rho_f {V_f^\alpha}^2 \ , \tag{2}$$

where C_d^α and C_l^α are the drag and lift coefficients for an ellipsoid with inclination α, respectively; $S_{ep}=\frac{\pi}{4}\varnothing_{eq}^2$ is the projected surface of the equivalent sphere of diameter $\varnothing_{eq}=\frac{6\Omega}{\pi}^{1/3}$, where $\Omega = \frac{4}{3}\pi abc$ is the volume of the ellipsoid, and V_f^α is the value of mean velocity in the horizontal direction around the grain. To consider the particle inclination in the computation of the drag, we use, according to [5], a combination of the drags for flow normal $C_d^{0^\circ}$ and for flow parallel $C_d^{90^\circ}$ to the mayor axis of the ellipsoidal particle,

$$C_d^\alpha = C_d^{0^\circ} + (C_d^{90^\circ} - C_d^{0^\circ})\sin^3\alpha \tag{3}$$

where:

$$\begin{aligned} C_d^{0^\circ} &= \frac{8}{Re}\frac{1}{\sqrt{\Phi_l}} + \frac{16}{Re}\frac{1}{\sqrt{\Phi}} + \frac{3}{\sqrt{Re}}\frac{1}{\Phi^{3/4}} + 0.4210^{0.4(-\log\Phi^{0.2})}\frac{1}{\Phi_c} \\ C_d^{90^\circ} &= \frac{8}{Re}\frac{1}{\sqrt{\Phi_c}} + \frac{16}{Re}\frac{1}{\sqrt{\Phi}} + \frac{3}{\sqrt{Re}}\frac{1}{\Phi^{3/4}} + 0.4210^{0.4(-\log\Phi^{0.2})}\frac{1}{\Phi_l} \ . \end{aligned} \tag{4}$$

Symbols $\Phi=S_{eq}/S$, $\Phi_l=S_{ep}/(S/2-S_{lp})$, and $\Phi_c=S_{ep}/S_{tp}$ are the sphericity, the lengthwise sphericity, and the crosswise sphericity, respectively. The surface of the equivalent sphere is given by $S_{eq}=\pi\varnothing_{eq}^2$, S is the surface of the ellipsoid, calculated by the approximate formula of [4] $S \approx 4\pi((a^pb^p + a^pc^p + b^pc^p)/3)^{1/p}$ where p=1.6075, and $S_{lp}=\pi ac$ is the surface obtained by the longitudinal projection of the surface of the ellipsoid. $S_{tp}=\pi bc$ is the surface obtained by the transversal projection of the surface of the ellipsoid. According to Ref. [5], lift coefficient is given by:

$$C_l^\alpha = C_d^\alpha \sin^2\alpha\cos\alpha \ . \tag{5}$$

Values of Reynolds number in the drag and lift coefficients of Eqs. (4) are those corresponding to the (volume equivalent) sphere, $Re = \rho_f V_f^\alpha \varnothing_{eq}/\nu$, where ν is the dynamic viscosity of the fluid.

2.1 Velocity field and threshold stress

This subsection describes the computation of the mean velocity of the flow around an ellipsoidal particle V_f^α and the relation for critical threshold shear stress $\tau^\star$ as a function of friction Reynolds number $Re^\star$ of a single particle, for different relations of proportionality of the semi–axes f and inclinations α. The mean velocity is computed with the following expression $V_f^\alpha = \dfrac{1}{S_p^\alpha}\displaystyle\int_{S_p^\alpha} u(y,z)dS'$. Where $u(y,z)$ is the velocity of the flow at point y, z, $S_p^\alpha = \pi b p_y/2$ is the area of a ellipse obtained as the projection of the inclined ellipsoid on a plane perpendicular to the flow. Figure 3 depicts the geometrical meaning of p_y, magnitude vertical axis of the ellipse defined as the distance between the two horizontal tangents to the ellipsoid at the highest and lowest points, see also Fig. 4 for a detailed representation of the flow around the ellipsoid.

$$p_y = 2(a\cos\phi_b \sin\alpha + b\sin\phi_b\cos\alpha) \tag{6}$$

The relation for critical threshold shear stress $\tau^\star$ as a function of friction Reynolds number

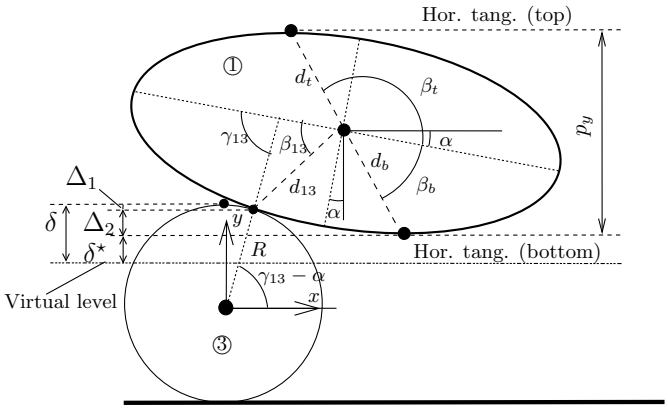

Figure 3: Vertical projection p_y, position of the virtual level δ and position $\delta^\star$ of the bottom of the particle respect to δ

$Re^\star$ of a single particle, requires the definition of $Re^\star = u^\star \varnothing_{eq}/\nu$ (different of the particle Reynolds number Re), where $u^\star = \sqrt{\tau/\rho_f}$ is the friction velocity, and τ is the wall shear stress. To determine threshold stress $\tau^\star = \tau/((\rho_s - \rho_f)g\varnothing_{eq}) = u^{\star 2}\rho_f/((\rho_s-\rho_f)g\varnothing_{eq})$, low friction Reynolds number regime and high friction Reynolds number regime must be discriminated to calculate the corresponding drag and lift forces.

For low friction Reynolds number (about $Re^\star$<1), the flow is laminar and the velocity distribution around the particle is linear $\frac{u(y,z)}{u^\star} = \frac{yu^\star}{\nu}$ (see left profile of Fig. 4), and the mean velocity is:

$$V_f^\alpha = \frac{1}{S_p^\alpha}\int_{y=\delta^\star}^{y=\delta^\star+p_y} \frac{yu^{\star 2}}{\nu} 2z(y)dy = \frac{p_y u^\star}{\nu} \tag{7}$$

where $dS' = 2z(y)dy$ is the differential area of the projected ellipse and

$$z(y) = \sqrt{b^2 \left(1 - \frac{4(y - p_y/2)^2}{p_y^2}\right)} \ ,$$

(see the right of Fig. 4 for details). The $\delta^\star$ is the distance between the virtual level (zero

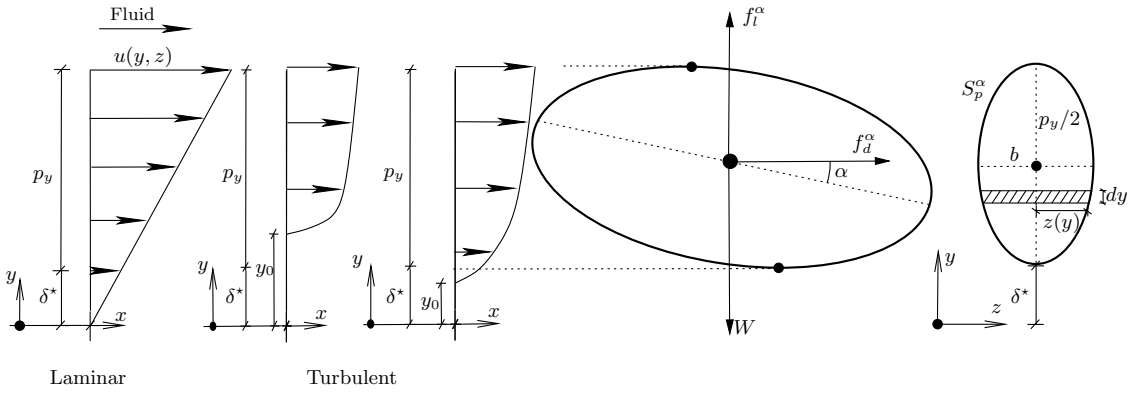

Figure 4: Velocity distribution for low particle Reynolds number (left profile) and high Reynolds number (intermediate and right profile).

velocity level) and the lowest point of the ellipsoid, while δ is the distance from the top level of the bed of the particles to the virtual level and is obtained from the geometry shown in Fig. 3.

For large particle friction Reynolds number ($Re^\star \geq 30$), the flow is turbulent and the velocity distribution around the particle (middle and right profiles of Fig. 4) is

$$\frac{u(y,z)}{u^\star} = \frac{1}{\kappa} \log \frac{y}{y_0} \approx 2.5 \log \frac{y}{y_0} \ ,$$

where κ=0.41 is the von Karman constant and z_0 is an equivalent bed roughness length (usually taken as $R/30$ to $R/10$, where R is the radius of cylinders on the bottom bed [8]). Mean velocity is computed as

$$V_f^\alpha = \frac{1}{S_p^\alpha} \int_{S'} u(y,z) dS' = \frac{1}{S_p^\alpha} \int_{S'} \frac{u^\star}{\kappa} \log\left(\frac{y}{y_0}\right) dS' = \frac{1}{S_p^\alpha} \int_{y=\varepsilon}^{y=\delta^\star + p_y} \frac{u^\star}{\kappa} \log\left(\frac{y}{y_0}\right) 2z(y) dy \ . \tag{8}$$

Depending on the location of the particle respect to the zero velocity level, the lower limit of the integral is ε=y_0 if $\delta^\star < y_0$ or ε=$\delta^\star$ if $\delta^\star \geq y_0$ (see middle and right profiles of Fig. 4, respectively). The above integral has to be evaluated numerically since there is not

an explicit analytical expression. By combining Eqs. (1) with Eqs. (2) values of V_f^α that initiates each kind of motion for laminar and turbulent regimes are given by

$$\frac{C_d^\alpha}{2} S_{ep} \rho_f {V_f^\alpha}^2 = (|\boldsymbol{W}| - \frac{C_l^\alpha}{2} S_{ep} \rho_f {V_f^\alpha}^2) K_i \; ; \quad i = r, s, sc \tag{9}$$

where C_d^α and C_l^α also depend on V_f^α through Re. Finally, by inserting equation (7) into (9) three non–linear equations yields to $u^\star$ for initiation of motion for rolling and slidings in the laminar regime. Three additional equations are obtained for the turbulent regime inserting Eq. (8) into Eq. (9). The whole set of six equations enables to compute $u^\star$ and therefore the relation $Re^\star$–$\tau^\star$ for the three kind of motions and for the two regimes.

3 Discrete element method

The DEM is a numerical method suitable for simulating the interaction among particles by frictional contacts. The non–penetration condition between particles i and k is imposed by a gap function $g_N^{ik}(\boldsymbol{X}) = \big[\boldsymbol{X} - \boldsymbol{Y}(\boldsymbol{X})\big]\ \boldsymbol{n}^{ik} \geq 0$ that measures the minimum distance between the contours of the particles. The points $\boldsymbol{X}$, $\boldsymbol{Y}$ define the coordinates of the set of points belonging to i and k respectively, that are either in contact, or in the closest position to the opposite body, and $\boldsymbol{n}^{ik}$=$-\boldsymbol{n}^{ki}$ is the normal unit vector at contact point (see Fig. 5). The aforementioned points and vector for ellipsoidal and spherical particles are obtained following the procedure of Ref. [9]. To describe the motion of contact points in the tangential direction it is necessary to add a kinematic condition by introducing the tangential gap g_T^{ik} as follows, $g_T^{ik}(\boldsymbol{X}) = \big[\boldsymbol{X} + \boldsymbol{\epsilon}^i(\boldsymbol{X}) - \boldsymbol{Y}(\boldsymbol{X}) - \boldsymbol{\epsilon}^k\big(\boldsymbol{Y}(\boldsymbol{X})\big)\big]\ \boldsymbol{t}^{ik}$, where $\boldsymbol{\epsilon}^i(\boldsymbol{X})$ and $\boldsymbol{\epsilon}^k\big(\boldsymbol{Y}(\boldsymbol{X})\big)$ are the displacements of the contact points defined as $\boldsymbol{X}$ in body i and $\boldsymbol{Y}(\boldsymbol{X})$ in body k, respectively. The displacements correspond to a time increment Δt and $\boldsymbol{t}^{ik}$ is the tangential unit vector at contact point (see Fig. 5).

To prescribe non–penetration dinamically the method imposes contact force defined as

$$\boldsymbol{f}_c^{ik} = |\boldsymbol{N}_{ik}|\ \boldsymbol{n}^{ik} + |\boldsymbol{f}_{r\,ik}|\ \boldsymbol{t}^{ik}\ ,$$

where N_{ik} and $f_{r\,ik}$ are the components of contact force in normal and tangential direction. In case of two rigid rounded bodies, contact force is applied at a single point. The contact force is modeled by penalization techniques (e.g. [6] and references therein). The key idea is to introduce two parameters, denoted as K_N and K_T, representing two high stiffness elastic springs placed between the contact points of the bodies along normal and along tangential directions respectively (see right Fig. 5). Hence, contact forces are: $|\boldsymbol{N}_{ik}| = K_N g_N^{ik}$ and $|\boldsymbol{f}_{r\,ik}| = K_T g_T^{ik}$ (rolling), or $|\boldsymbol{N}_{ik}| = K_N g_N^{ik}$ and $|\boldsymbol{f}_{r\,ik}| = \mu\,|\boldsymbol{N}_{ik}|$ (sliding).

Governing equations of a set of $\mathtt{n}_{bd}$ interacting bodies are formulated by Hamiltonian mechanics and are numerically solved by the discrete element method. The formulation results in the following equations of motion for each body:

$$\dot{\boldsymbol{Q}}^i = \frac{\boldsymbol{P}^i}{\rho_{sol}}; \quad \dot{\boldsymbol{P}}^i = -\nabla V\big(\boldsymbol{Q}^i\big); \quad i = 1, \ldots, \mathtt{n}_{bd}, \tag{10}$$

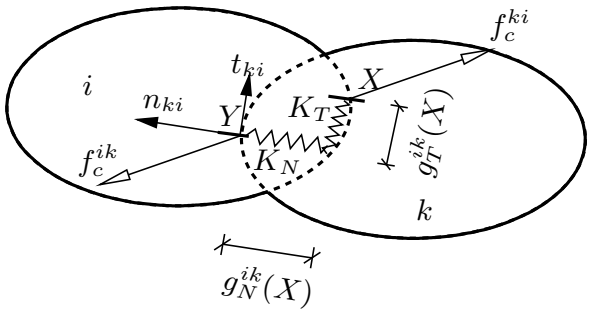

Figure 5: Left: Contact between two bodies. Right: g_N^{ik} defines the maximum penetration, g_T^{ik} defines the tangential displacement.

where $\boldsymbol{Q}^i(x, y, t)$ is the position of the particle i, $\boldsymbol{P}^i(x, y, t)$ is the linear momentum of the particle i. We approximate Eqs. (10) by a discrete representation of displacements (x,y displacements and rotation) and linear momentum (x, y and angular momentum) with first order nodal shape functions contained in the 2×3 matrix $\boldsymbol{\mathcal{N}}^i(x, y)$ such that for each body i,

$$\boldsymbol{Q}^i = \boldsymbol{\mathcal{N}}^i \boldsymbol{q}^i; \;\; \boldsymbol{P}^i = \boldsymbol{\mathcal{N}}^i \boldsymbol{p}^i \; . \tag{11}$$

Here $\boldsymbol{q}^i$ and $\boldsymbol{p}^i$ are values of displacements and momenta at the centroid of the particle. By replacing the discretization given by Eqs. (11) into Eqs. (10), we accomplish:

$$\dot{\boldsymbol{q}} = \boldsymbol{M}^{-1} \boldsymbol{p} \; ; \qquad \dot{\boldsymbol{p}} = \boldsymbol{f}_c + \boldsymbol{f}_d + \boldsymbol{f}_l + \boldsymbol{W} \; , \tag{12}$$

where $\boldsymbol{M}$ is the assembled lumped mass matrix. Time integration of Eqs. (12) is performed by an implicit one step algorithm proposed in [2].

4 Experiments

A set of simulations are conducted for a single ellipsoidal inclined particle of non–cohesive sediment resting in an horizontal bed to obtain the relation between $Re^\star$ and $\tau^\star$. The beds are composed of fixed cylinders of the same radius as the semiaxis a of the ellipse. The analytical and numerical computations are compared with the experimental results and are defined taking into account the non full sphericity of the grains.

4.1 Incipient motion

Both numerical and analytical experiments consider the configuration depicted in Fig. 1 (right). To restrict the motion of the particles on the bottom in the numerical computation, a high friction coefficient is imposed by the lateral boundaries. We assume that evolution of particles on the bottom do not modify substantially the velocity field. Parameters for the particles and flow are: density of the particles ρ_{sol}=2500 kg/m^3, particle friction angle ϕ=15°, friction between particles and lateral boundaries ϕ=40°, density of flow ρ_f=1 kg/m^3 (air), kinematic viscosity ν=10^{-5}m^2/s, and g=9.81 m/s^2. The relation

$Re^\star - \tau^\star$ is obtained by solving the succesive scaling of the model (Fig. 1), ranging from laminar to turbulent regimes. We compute a value of $u^\star$ and then $Re^\star$, $\tau^\star$, for each scale. For DEM, the $Re^\star$, $\tau^\star$ relationship is also obtained by scaling the set of particles and by gradually increasing the flow. Computation of the evolution of particles by the DEM assumes that motion occurs once particle overpasses the particle located on the bottom right. In case that this limit is not reached, $u^\star$ is progressively increased. Same procedure is repeated for sets of particles of different size. The numerical parameters for DEM are: time increment for integration of Eqs. (12) is Δt=0.0025 s, and K_N=K_T=10^6 N/m. A minimum value of the large semiaxis is a=5×10^{-5}m is adopted to avoid ill–conditioning problems. To simulate very small $Re^\star$ conditions, fluid viscosity is augmented (ν=10^{-3}m^2/s).

Figures 6 to 8 show the relation $Re^\star - \tau^\star$ (Shields diagram) for $f = 1.0, 0.75$ and 0.5, and inclinations $\alpha = 0, 15, 35°$. In the figures two regions can be clearly identified, the low particle friction Reynolds number region (left), and the high particle friction Reynolds number region (right). Between both regions, a range defined approximately as $4<Re^\star<30$ specifies a transition, where the representation of drag and lift given by Eq. (2) is not adequate. For very low friction Reynolds numbers ($Re^\star<1$) the stress decreases as the $Re^\star$ increases, and the force exerted by the flow also increases due to the viscosity forces. The opposite case is for high $Re^\star$ range, where the pressure force is higher than viscous force and initiation of motion requires a higher stress.

In general, a variation in α and f produces a substantial variation in the stress. For $\alpha = 0°$ (Fig. 6) the particle is exposing the minimum area to the action of the flow and consequently it is expected the highest stress. For $f = 1$ (sphere), the motion is by rolling since it corresponds to the lowest stress. As f decreases, the mode of motion changes from rolling to sliding. Notice that for $f = 0.75$ the stress for the three kinds of motion coincides. For $f < 0.75$, stress to produce motion by rolling increases and stress for sliding decreases, since the mechanical arm of the particle decreases as f decreases (see the right Fig. 6). Therefore, the force induced by the flow is lower to produce sliding than to produce the moment to roll the particle. For the laminar range the stress decreases for $f = 0.50$, due to the low weight of the particle that reduces the resistant force of the motion.

DEM reproduces the analytical results. Notice that the numerical results do not always correspond to the lowest stress. Figures 6 to 8 right show that motion computed by DEM is produced by the intermediate stress, that corresponds to sliding where the particle has only one contact (special case). Experimental and numerical results frequently show that initiation of motion is produced while one contact is maintained. Numerical and analytical results fit well with the experimental limits [7], for spherical particles or particles with $f = 0.75$ for all inclinations. For $f = 0.50$ the numerical results are within or closer to the experimental limits for $\alpha = 35°$.

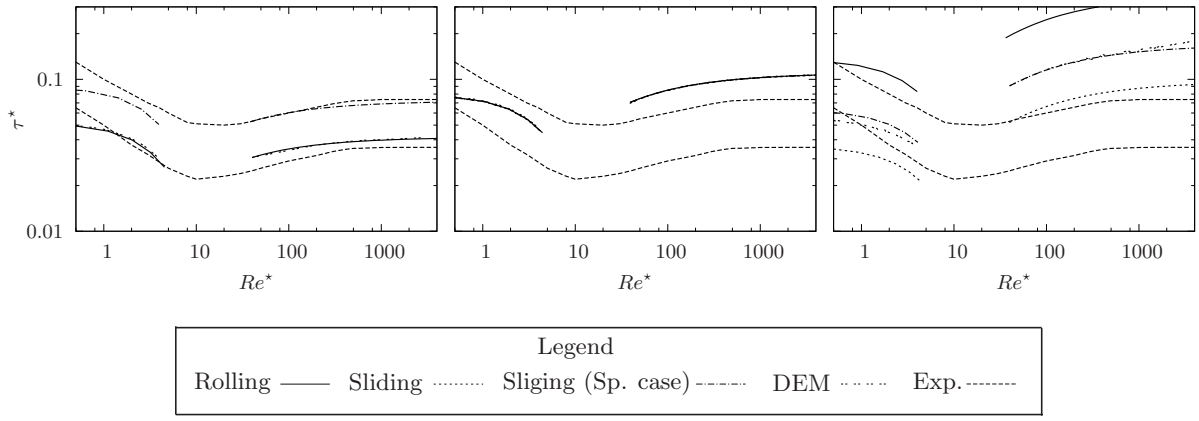

Figure 6: $Re^\star$, $\tau^\star$ relation for $\alpha = 0°$ and $f = 1.0$, 0.75, 0.50, left to right respectively.

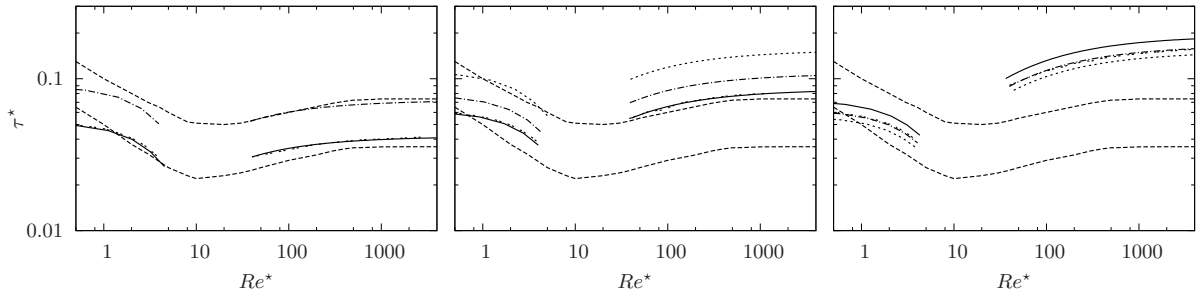

Figure 7: $Re^\star$, $\tau^\star$ relation for $\alpha = 15°$ and $f = 1.0$, 0.75, 0.50, left to right respectively.

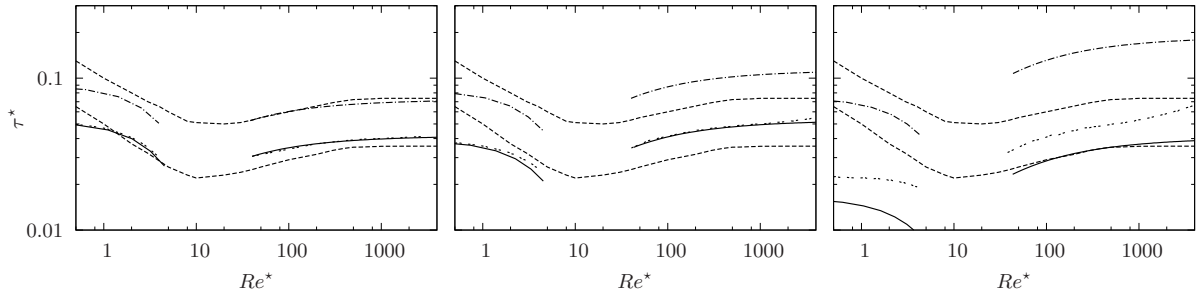

Figure 8: $Re^\star$, $\tau^\star$ relation for $\alpha = 35°$ and $f = 1.0$, 0.75, 0.50, left to right respectively.

5 Conclusions

The initiation of motion of an ellipsoidal particle that rests on a sediment bed has been analyzed using new analytical and numerical (DEM) approaches. The new approaches consider a variety of shapes and orientations that previous formulations do not take into account. Results show good agreement with the experimental results given by Shields, particularly with the dispersion of lab results, where a wide shape variation exists. Extension for non–horizontal beds of this work is currently developed by the authors and will be pursued and reported in future publications.

6 Acknowledgements

This work was partially supported by the MICIIN Grant #BIA-2012-32918 and #BIA-2008-00522.

REFERENCES

[1] R. Bravo, P. Ortiz, and J.L. Pérez-Aparicio. Incipient sediment transport for non-cohesive landforms by the discrete element method (dem). *Applied Mathematical Modelling*, 38(4):1326–1337, 2014.

[2] R. Bravo, J. L. Pérez-Aparicio, and T. A. Laursen. An enhanced energy conserving time stepping algorithm for frictionless particle contacts. *International Journal for Numerical Methods in Engineering*, 2010.

[3] S. Dey. Sediment threshold. *Applied Mathematical Modelling*, 23(5):399–417, 1999.

[4] M.S. Klamkin. Elementary approximations to the area of n-dimensional ellipsoids. *American Mathematical Monthly*, 78:280–283, 1971.

[5] Matthias Mando and Lasse Rosendahl. On the motion of non-spherical particles at high reynolds number. *Powder Technology*, 202:1–13, 2010.

[6] J.L. Pérez-Aparicio and R. Bravo. Discrete elements. In Consorcio TCN, editor, *Practical Aplications Using Computational Contact Mechanics*, volume 2, 2006.

[7] A Shields. Application of similarity principles and turbulence research to bed-load movement. Technical report, Lab. for Hydraulic Water Resources, 1936.

[8] L.C. van Rijn. Sediment transport. part i: bed load transport. *Journal of Hydraulic Engineering-ASCE*, 110(10):1431–1456, 1984.

[9] C. Wellmann, C. Lillie, and P. Wriggers. A contact detection algorithm for superellipsoids based on a contact detection algorithm for superellipsoids based on the common-normal concept. *Engineering Computations (Swansea, Wales)*, 25(5):432–442, 2008.

[10] P.L. Wiberg and J.D. Smith. A theoretical model for saltating grains in water. *Journal of Geophysical Research*, 90:7341–7354, 1985.